

1 SUPPLEMENTAL MATERIAL

2 Supplemental methods

3 **Immunofluorescence staining**

4
5
6
7 Embryos and pups were fixed in 2% fresh paraformaldehyde (PFA) solution in PBS
8 overnight rocking at 4°C, washed in PBS, cryoprotected in sucrose solutions, embedded
9 in optimum cutting temperature (OCT) embedding compound (Tissue-Tek), and frozen
10 at -80°C. Tissue sections were first incubated with blocking buffer (10% donkey serum,
11 0.1% Triton X-100 and 1% BSA in PBS) for 1 hour at room temperature and then with
12 primary antibodies overnight at 4°C. The following primary antibodies were used: anti-
13 Cxcr4 (Abcam, ab124824), anti-Endomucin (Santa Cruz, sc-65495), anti-ER α (Santa
14 Cruz, sc-543), anti-Erg (Abcam, ab92513), anti-Fabp4 (Abcam, ab13929), anti-
15 GFP (Abcam, ab13970), anti-ICAM2 (BD Pharmingen 553326), anti-Unc5b (Cell
16 Signaling, 13851), anti-VeCadherin (BD Biosciences, 555289), and anti- α SMA-Cy3
17 (Sigma, C6198). Alexa fluor-conjugated secondary antibodies (Invitrogen) were
18 incubated for 1-2 hours at room temperature to detect the signals. For some weak
19 signals, HRP-conjugated secondary antibodies and tyramide signal amplification kit
20 (PerkinElmer) were used to magnify the signals. Sections were mount with Vectashield
21 (Vector). All images were captured on a Zeiss LSM-780 confocal microscope. ImageJ
22 software was used as image analysis tool.

23 **Three-dimensional imaging**

24
25
26 Clearing of the dissected embryonic or postnatal hearts were performed with an adapted
27 iDISCO protocol⁵⁹.

28 Embryonic or postnatal hearts were dissected from the body and fixed in fresh 2% PFA
29 overnight at 4°C and then thoroughly washed with PBS. Permeabilization was performed
30 with PBT 0.2% for 2h, and then with PBS/0.1% Tween20/0.1% TritonX-100/0.1%
31 Deoxycholate/0.1% NP40/20% DMSO overnight at room temperature. Samples were
32 then blocked with blocking buffer (PBS/0.2%TritonX-100/10%DMSO/0.3Mglycine/6%
33 Donkey) Serum for 12h at room temperature and washed with PBTwH(PBS/0.2%
34 Tween-20 with 10ug/ml heparin) 1h. The incubation of primary antibody was performed
35 in PBTwH / 5% DMSO/ 3% Donkey Serum, shaking for 24h at room temperature. The
36 antibodies used were the same antibodies used for immunofluorescence on sections.
37 The concentration of the primary antibody was 1:25-1:200 depending on the sample size.
38 Afterwards, hearts were washed with PBTwH 1h shaking at room temperature eight
39 times. Alexa Fluor-conjugated secondary antibodies were incubated in PBTwH/3%
40 Donkey Serum overnight shaking at room temperature, at a concentration of 1:50-1:200
41 depending on the sample size. After thoroughly washing samples with PBTwH again 1h
42 shaking at room temperature eight times. For clearing, samples were dehydrated with
43 increasing concentrations of Tetrahydrofuran solution in H₂O (THF): 1h in THF 50%, 1h
44 THF 80% and two times 1h THF 100%, and then in Dichloromethane until samples sink
45 at the bottom (with a maximum of 5 minutes). Finally, samples were cleared in DiBenzyl
46 Ether (DBE) shaking until the sample was clear. Samples can be stored in DBE at 4°C
47 until imaged.

48 For imaging, samples were placed in a drop of DBE on a glass-bottomed dish. Image
49 acquisition was performed with a long working-distance oil-immersion 25x objective on
50 a Zeiss LSM-780 microscope. Z-stacks of a maximum of 460um were acquired. For
51 samples bigger than E12, two different z-stacks acquisition were performed, one from
52 de dorsal side of the heart, and the other from the ventral side.

53 **Three-dimensional images post-processing**

56 After confocal images acquisition, Zen 3.4 Blue edition software (Zeiss) was used for
57 stitching. Arivis Vision4D software (Zeiss) was used for registering dorsal and ventral Z-
58 stacks when needed. ImageJ was used for manual segmentation. Imaris 9.9.0 (Oxford
59 Instrumentals) was used for three-dimensional rendering, colocalization analysis and
60 area quantification.

61 The segmentation of the coronary plexus or the endocardium was performed manually.
62 Navigation through z-stacks of confocal images allowed to determine whether a cell or
63 vessel is in continuation to the subepicardial plexus or, in contrast, is still integrated within
64 the endocardium. The higher intensity of Endomucin staining shown by endocardial cells
65 also served to identify whether a sprouting cell remained connected to the endocardial
66 lining. In those cases of connections of endocardium and coronary plexus, the
67 segmentation boundary was decided arbitrary, by extrapolating the limit between
68 endocardium and coronary plexus of neighbor cells.

69

70 **Live imaging on explanted hearts**

71

72 Live-imaging on explanted embryonic heart was performed as previously described⁴³.
73 E12.5 *PdgfbCreERT;R26mTmG* embryos were dissected in PBS supplemented with
74 10%FBs, penicillin (100 U/ml) and streptomycin (100ug/ml). Hearts were isolated and
75 transferred to HEPES-buffered DMEM/F12 medium supplemented with 2% FBS and
76 penicillin-streptomycin. Hearts then were embedded into a 0.5% low melting point
77 agarose gel (Sigma-Aldrich) in a glass-bottomed culture dish (MatTek) and bathed in the
78 same medium used for heart dissection. Images were captured in a 3i spinning-disc
79 confocal microscope every 10 min for 15 hours. During image capture the culture
80 chamber was maintained at 37 °C in a 5% CO₂ humidified atmosphere.

81

82 **Single cell suspension preparation and cell sorting**

83

84 Single-cell suspension of ECs was prepared as described previously⁶⁰. C57Bl6 8 weeks
85 old adult animals, P2 postnatal, E15 and E12 were used for single-cell suspension
86 preparation. Adult animals were sacrificed by cervical dislocation while embryonic and
87 postnatal animals were decapitated. Adult and postnatal hearts were chopped with a
88 scalpel until getting 1-2mm pieces of tissue. The enzymatic digestion was adapted to
89 every stage analyzed: for E12, 20min of Collagenase/Dispase (Sigma-Aldrich) (1mg/ml),
90 for E15, 30min of Collagenase/Dispase (1mg/ml), and for P2 and adult hearts, 20 min of
91 Collagenase II (500units/ml) (Worthington) plus a second digestion step with
92 Collagenase/Dispase for 30min. All steps were performed at 37°C, under agitation and
93 pipetting up and down the solution within the tubes every 5min. To stop the enzymatic
94 reaction 10ml of cold FAC buffer (HBSS/2%FBS/10mM HEPES) was added to the
95 samples and then spinned down (400G, 5 min). For adult samples, red blood cells lysis
96 step (Invitrogen) was performed. After enzymatic digestion, cell debris removal solution
97 (Miltenyi) was performed and finally, all suspension filtered through a 40um strainer.

98 Single-cell suspensions were incubated with primary antibodies in FACS buffer for 20
99 min on ice. The following antibodies were used: APC-conjugated anti-CD31 (Thermo
100 Fisher, 17-0311-80) and PE-conjugated anti-CD45 (BD Biosciences, 553081). Samples
101 were centrifuged (400G, 5 min) and resuspended on FACS buffer and stored on ice until
102 applied to the flow cytometer. CD31+/CD45- cells were sorted on an Aria II into 1.5ml
103 tubes with EBM2 media. Compensation controls were set up for each single channel.
104 After completion of sorting, 10% DMSO was added and cell suspension frozen at -80°C.
105 Several rounds of single-cell suspension preparation, sorting and freezing was repeated
106 for embryonic samples in order to get a significant number of cells: 8 weeks old adult
107 animals (n=6), P2 postnatal (n=21), E15 (n=48) and E12 (n=37).

108 Frozen vials of sorted CD31+/CD45- cells from E12, E15, P2 and 8wo adult hearts were
109 thawed in a water bath at 37°C. For E12 and E15, a dead cell removal kit (Miltenyi) was

110 applied. For P2 and adult, re-sorting by flow cytometry and selection of live cells was
111 performed.

112

113 **Library preparation and 10X Chromium sequencing**

114

115 Cell suspension was adjusted to 400-1000 cells per microliter and loaded on the
116 Chromium controller (10X Genomics) with a targeted cell recovery of 8000-10000 per
117 reaction. 3' gene expression libraries were prepared according to the manufacturer's
118 instructions of the v2 Chromium Single Cell Reagent Kits (10X Genomics). Quality
119 control of cDNA and final libraries was done using Bioanalyzer 2100 (Agilent). Libraries
120 were sequenced using HiSeq 4000 (Illumina) targeting a depth of 25000 reads per cell.

121

122 **Transcriptome mapping**

123

124 After sequencing, the sequence data were mapped to the mouse reference genome
125 (mm10 pre-build references v 2.1.0) provided by 10X Genomics using the CellRanger
126 suite (v.2.2). The count matrices generated by CellRanger as followings were used for
127 further analysis. Mapping quality was assessed using the CellRanger summary statistics.

128

129 **Empty droplets removal and doublet estimation**

130

131 Empty droplets were identified by Emptydrops, which is implemented in the CellRanger
132 workflow. After removal of empty droplets, we applied scrublet per sample⁶¹ to assign a
133 doublet score (scrublet_score) to the metadata container of each cell.

134

135 **Cell quality control and filtering**

136

137 Downstream analysis employed the concatenated filtered feature-barcode matrices,
138 using Seurat⁶². Genes were filtered out when they were expressed in less than three
139 cells. The filtering cut-off was decided based on the distribution of data quality and the
140 estimated doublet ratio provided by 10X Genomics. We applied individual cell filtering
141 criterion: cells from E12 were filtered for counts (nCount_RNA <= 4000), genes
142 (nFeature_RNA <= 1500), mitochondrial genes (percent.mt <= 10%), and scrublet score
143 (scrublet_score <= 0.15). Cells from E15 were filtered for counts (nCount_RNA <= 3000),
144 genes (nFeature_RNA <= 1300), mitochondrial genes (percent.mt <= 10%), and scrublet
145 score (scrublet_score <= 0.15). Cells from P2 were filtered for counts (nCount_RNA <=
146 12000), genes (nFeature_RNA <= 4000), mitochondrial genes (percent.mt <= 20%), and
147 scrublet score (scrublet_score <= 0.15). Cells from Adult were filtered for counts
148 (nCount_RNA <= 5000), genes (nFeature_RNA <= 2000), mitochondrial genes
149 (percent.mt <= 20%), and scrublet score (scrublet_score <= 0.15).

150

151 **Cell cycle score calculation**

152

153 Cell cycle score were calculated using CellCycleScoring function integrated in Seurat.
154 Previously reported cell cycle genes⁶³ are used for the reference of cell cycle genes after
155 converting the human gene list into mouse orthologues using biomaRt (v2.52.0).

156

157 **Dimensionality reduction, clustering, and analysis of differentially expressed genes**

158

159 After read count normalization and log2-transformation, top 2000 highly variable genes
160 were selected. Then, regression of UMI counts, percent mitochondrial gene expression
161 and cell cycle gene expression was performed. Prior to manifold construction using
162 UMAP, top 30 principal components were harmonized by anchored canonical correlation
163 analysis (CCA)⁶⁴. Cells were clustered using the original Louvain algorithms⁶⁵. For all

164

165 datasets, non-endothelial subtypes (e.g. blood and immune cells, cardiomyocytes,
166 smooth muscle, fibroblasts) as well as a small number of lymphatic cells were removed.
167 Likewise, immediate early genes-expressing cells were also removed as considered
168 stressed cells during the single-cell suspension preparation process.
169 DEGs of each cluster were calculated using FindAllMarkers function of Seurat with the
170 Wilcoxon rank sum test. For the marker gene computation, we selected genes expressed
171 in at least 25% of cells in either of the populations and with a log2-transformed fold
172 change of at least 0.25. Genes with adjusted p-value < 0.05 were called as DEGs.

173

174 **Left anterior descending coronary artery ligation (LAD)**

175

176 Myocardial infarction (MI) was induced in mice through the ligation of the left anterior
177 descending (LAD) coronary artery on 8-12 weeks C57Bl6/J mice. Prior to surgery, mice
178 were anesthetized using vaporized isoflurane, intubated with a 20G intravenous
179 catheter, and placed on a mechanical ventilator for respiratory support. Additionally, to
180 prevent hypothermia, animals were positioned on a heating pad to maintain body
181 temperature throughout the procedure. The surgical site was prepared by performing a
182 left thoracotomy at the fourth-fifth intercostal space, allowing access to the heart.
183 Subsequently, muscles overlying the chest cavity were dissected to expose the LAD
184 coronary artery. Using a 7/0 non-absorbable ethylene suture, the LAD artery was
185 permanently ligated, ensuring complete occlusion. Verification of successful ligation was
186 confirmed visually by observing anemia and akinesis of the apex and anterior-lateral
187 wall. Following the confirmation of coronary occlusion, the thoracic cavity was closed in
188 layers to minimize the risk of post-operative complications. Upon completion of the
189 surgery, mice were extubated and monitored closely until fully recovered. To facilitate
190 recovery, mice were kept warm and provided with appropriate post-operative care. Both
191 healthy and 3 days post-infarcted mice were sacrificed and subjected to fixation and
192 subsequent immunostaining.

193

194 **Integration of single-cell transcriptomic available data from control and 7dpi** 195 **cardiac endothelium**

196

197 Publicly available datasets were obtained from the Gene Expression Omnibus (GEO)
198 repository GSE132880⁴⁹. Single-cell RNA seq was performed on FACs sorted CD31+
199 Confetti+ Podoplanin- cell populations from four control and four 7dpi adult mouse hearts
200 from *PdgfbCreERT2;Rosa26Brainbow2.1*.

201 Downstream analysis employed the concatenated filtered feature-barcode matrices,
202 using Seurat⁶². Cells with >0.01 and >0.95 percentiles of nCount and nFeature and
203 >10% mitochondrial genes (percent.mt) were filtered out. Following data filtering,
204 datasets (E12, E15, P2, Adult, Control and 7dpi) were merged to create a unified
205 dataset for downstream analysis. The merged dataset underwent SCT normalization,
206 top 2000 highly variable genes selected and regression of percent mitochondrial gene
207 expression was performed. Integration of datasets was performed using Harmony. Prior
208 to manifold construction using UMAP, top 40 principal components were harmonized by
209 anchored canonical correlation analysis (CCA)⁶⁰. Cells were clustered using the original
210 Louvain algorithms⁶¹. Following already described criteria, non-endothelial subtypes
211 (e.g. blood and immune cells, cardiomyocytes, smooth muscle, fibroblasts, lymphatic
212 cells and immediate early genes-expressing cells were removed. DEGs of each cluster
213 were calculated using FindAllMarkers function of Seurat with the Wilcoxon rank sum test.
214 For the marker gene computation, we selected genes expressed in at least 25% of cells
215 in either of the populations and with a log2-transformed fold change of at least 0.25.
216 Genes with adjusted p-value < 0.05 were called as DEGs.

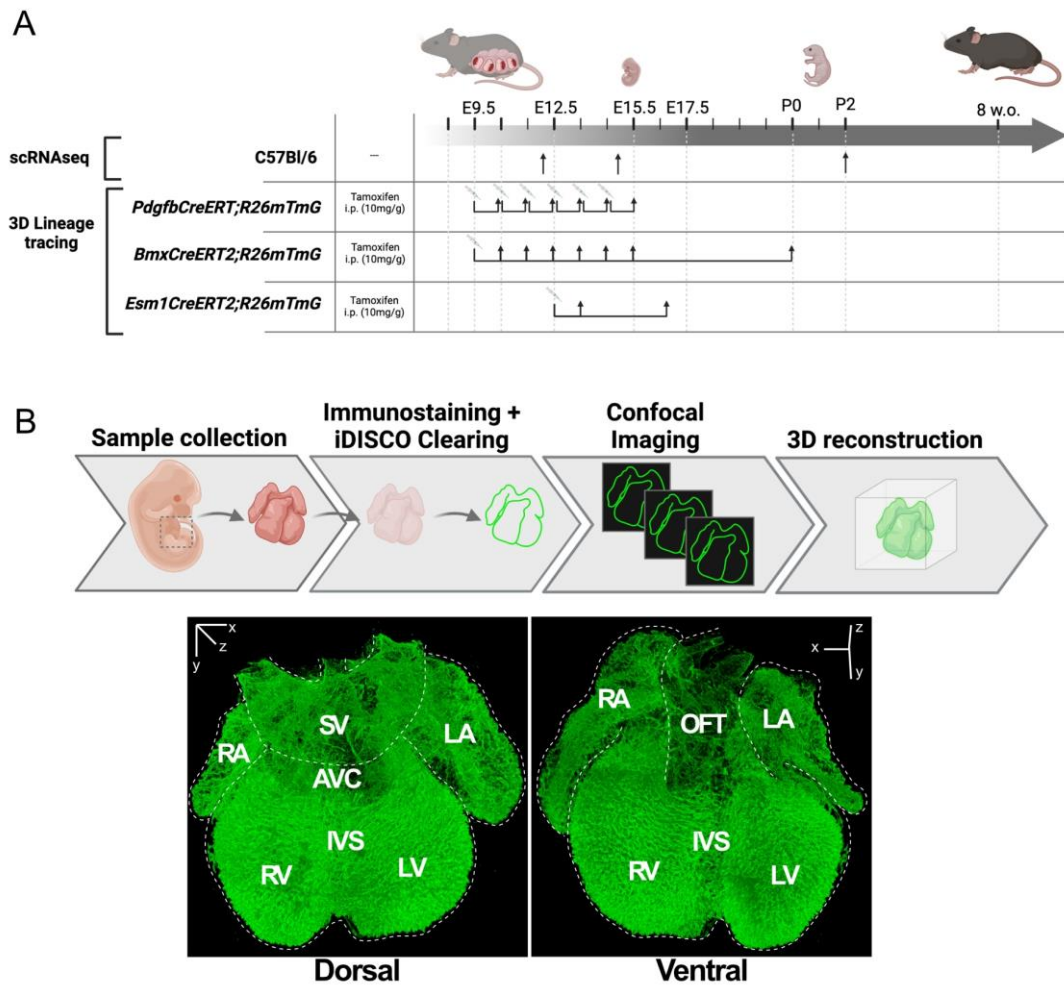
217

218 **Analysis of single-cell transcriptomic available data of human cardiac embryonic** 219 **endothelium**

220
221
222
223
224
225
226
227
228
229
230
231
232
233
234
235
236
237
238
239
240
241
242
243
244
245
246
247
248
249
250
251
252
253
254
255
256
257
258
259
260
261
262
263
264
265
266
267
268
269
270
271
272
273
274

Publicly available datasets were obtained from the Gene Expression Omnibus (GEO) repository GSE195911⁵⁰. Single-cell RNA seq was performed on FACs sorted cardiac ECs isolated by FACS from ventricular tissue obtained from two human fetuses at 13 and 14 weeks of gestation.

Downstream analysis employed the concatenated filtered feature-barcode matrices, using Seurat⁶². Cells with >0.01 and >0.95 percentiles of nCount and nFeature and $>10\%$ mitochondrial genes (percent.mt) were filtered out. Following data filtering, datasets (13 and 14 weeks) were merged to create a unified dataset for downstream analysis. The merged dataset underwent SCT normalization, top 2000 highly variable genes selected and regression of percent mitochondrial gene expression was performed. Integration of datasets was performed using Harmony. Prior to manifold construction using UMAP, top 40 principal components were harmonized by anchored canonical correlation analysis (CCA)⁶⁰. Cells were clustered using the original Louvain algorithms⁶¹. Following already described criteria, non-endothelial subtypes (e.g. blood and immune cells, cardiomyocytes, smooth muscle, fibroblasts, lymphatic cells and immediate early genes-expressing cells) were removed. DEGs of each cluster were calculated using FindAllMarkers function of Seurat with the Wilcoxon rank sum test. For the marker gene computation, we selected genes expressed in at least 25% of cells in either of the populations and with a log₂-transformed fold change of at least 0.25. Genes with adjusted p value < 0.05 were called as DEGs.

275 **Supplemental figures**

276

277

Figure S1. Methods summary

278

A. scRNAseq and lineage-tracing strategy. Mouse strains, tamoxifen administration and analysis timepoints (arrows).

279

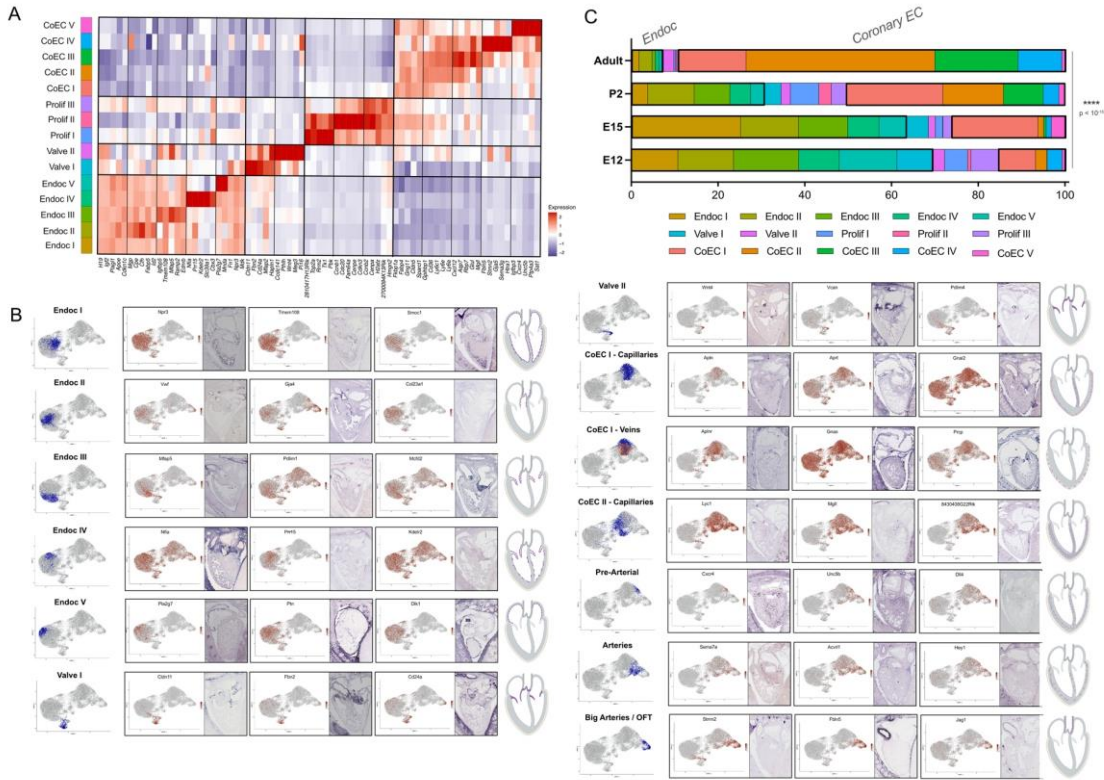
280

B. Three-dimensional imaging pipeline.

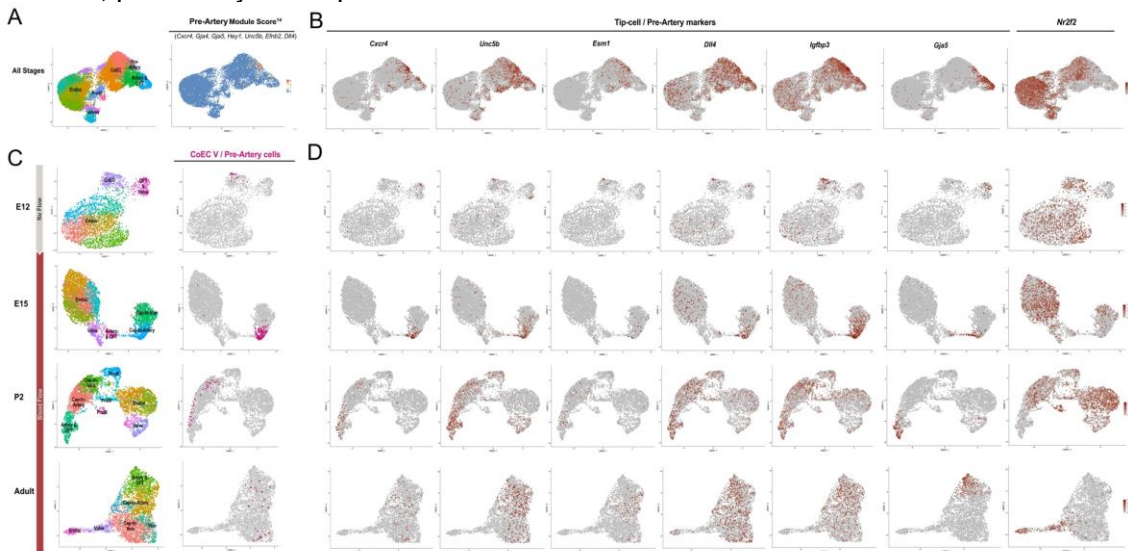
281

AVC=Atrioventricular canal; IVS=Interventricular septum; LA=Left atrium; LV=Left ventricle; OFT=Outflow tract; RA=Right atrium; RV=Right ventricle; SV=Sinus venous.

282

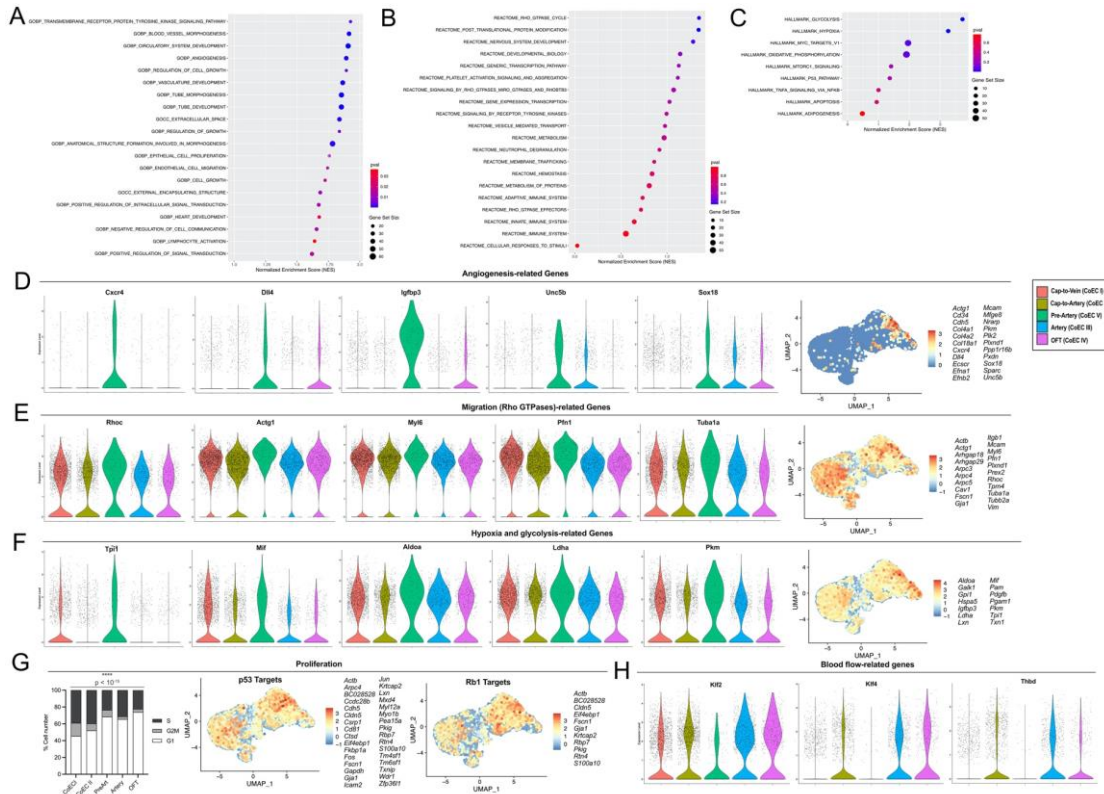


283
 284 **Figure S2. Validation of annotated clusters by *in situ* hybridization of top DEGs**
 285 **A.** Heatmap of top 5 marker genes of every annotated cluster.
 286 **B.** UMAP plot with every cluster highlighted in blue (left), panel with feature marker plots
 287 of three top marker genes of each cluster and corresponding ISH images from E14.5
 288 wildtype embryos (middle) and schematic of the observed signal in the ISH images
 289 (right). ISH images are from GenePaint database¹⁸.
 290 **C.** Percentage is calculated by cell number of every cluster, normalized to total cell
 291 number, p value by Chi-square test.



292
 293 **Figure S3. Tip cell signature of pre-arterial cells is stable throughout life.**
 294 **A.** UMAP of E12, E15, P2 and Adult integrated dataset and module score of previously
 295 described pre-arterial marker genes¹⁴.
 296 **B.** Feature marker plot of pre-arterial and tip cell markers (*Cxcr4*, *Unc5b*, *Esm1*, *Dll4*,
 297 *Igfbp3*), arterial marker (*Gja5*) and venous marker (*Nr2f2*) in the UMAP of the integrated
 298 datasets.

299 **C.** UMAP of individual datasets (first column) and mapping of pre-arterial cells annotated
 300 as CoEC V/ Pre-Artery in the integrated UMAP (second column, compare with fig. 1F).
 301 **D.** Feature marker plot of pre-arterial and tip cell markers (*Cxcr4*, *Unc5b*, *Esm1*, *Dll4*,
 302 *Igf1bp3*), arterial marker (*Gja5*) and venous marker (*Nr2f2*) in the UMAP of the individual
 303 datasets.
 304



305 **Figure S4. Pre-arterial cells show an angiogenic, migratory, glycolytic and low**
 306 **proliferative transcriptional profile.**

307 **A-C.** Gene set enrichment analysis of CoEC V/Pre-Artery cluster in comparison with the
 308 rest of CoEC clusters (CoEC I to CoEC IV) for GO-terms (A), reactome (B) and hallmarks
 309 (C).

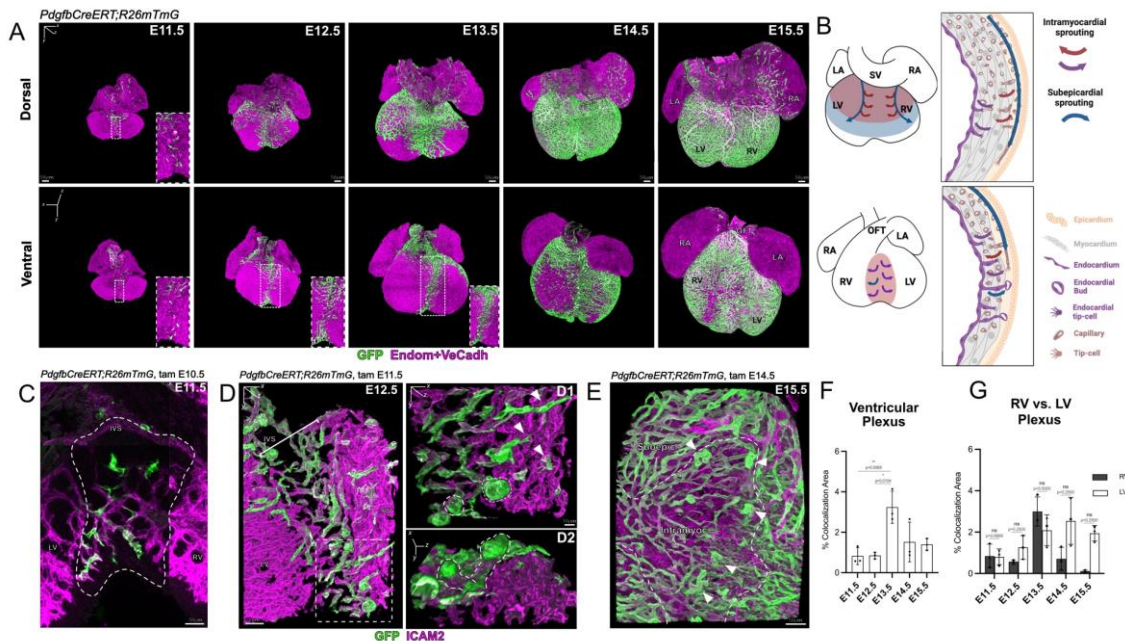
310 **D.** Violin plots of angiogenesis-related genes in all CoEC clusters and module score of
 311 all identified enriched genes of the corresponding GSEA. CoEC V/Pre-Artery cluster
 312 shows increased levels in comparison with other CoEC clusters.

313 **E.** Violin plots of Rho GTPases-related genes in all CoEC clusters and corresponding
 314 module score on the integrated UMAP. CoEC V/Pre-Artery cluster shows increased
 315 levels in comparison with other CoEC clusters.

316 **F.** Violin plots of hypoxia-related and glycolysis-related genes in all CoEC clusters and
 317 corresponding module score on the integrated UMAP. CoEC V/Pre-Artery cluster shows
 318 increased levels in comparison with other CoEC clusters.

319 **G.** Percentage of cells that are in G1, G2M and S cell cycle phase in each CoEC cluster.
 320 CoEC V/Pre-Artery cluster proliferation levels are reduced when compared with capillary
 321 cells and show similar levels to mature arteries (left). Percentage is calculated by number
 322 of cells categorized by cell cycle score algorithm (see methods), normalized to total cell
 323 number for every cluster of interest, p value by Chi-square test. Module score on the
 324 integrated UMAP of p53 and Rb1 targets found to be enriched in CoEC V/Pre-Artery
 325 cluster in comparison with the rest of the CoEC clusters.

326 **H.** Violin plots of blood flow-induced genes in all CoEC clusters. CoEC V/Pre-Artery
 327 cluster shows reduced levels in comparison with other CoEC clusters.
 328



329
330 **Figure S5. Distinct developmental sources with opposing sprouting directions**
331 **vascularize the myocardial walls.**

332 **A.** Three-dimensional rendering of E11.5-E15.5 *PdgfbCreERT;R26mTmG* hearts
333 stained against Endom+VeCadherin (magenta). Upper row shows dorsal view, lower row
334 shows ventral view.

335 **B.** Sprouting directions and sources of coronary plexus formation in dorsal and ventral
336 regions of the heart. At the dorsal side (upper row), the subepicardial plexus, which
337 originates at the SV, sprouts radially within the subepicardium to expand the plexus (blue
338 arrow), and tangentially towards the underlying myocardium to form the intramyocardial
339 plexus (red arrow). Simultaneously, endocardial cells sprout from the opposite direction
340 to also vascularize the myocardium (purple arrow). At the ventral side (lower row),
341 multiple individual endocardial cells sprout towards the myocardium. Few endocardial
342 cells that sprout directly into the subepicardium form bud-like structures. Both dorsal and
343 ventral plexus anastomose to close the network.

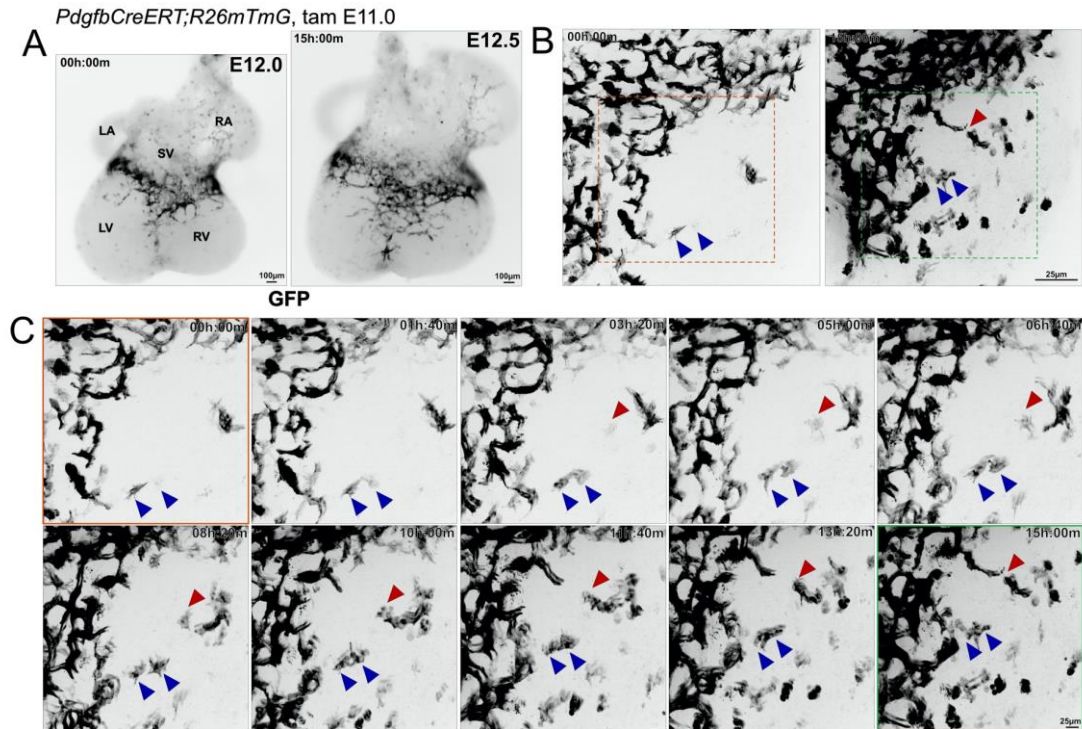
344 **C.** Three-dimensional rendering of the IVS region (dotted line) of a E11.5
345 *PdgfbCreERT;R26mTmG* heart stained against ICAM2 (magenta). *Pdgfb*-expressing tip
346 cells (green) are sprouting from the endocardium (magenta).

347 **D.** Three-dimensional rendering of the IVS region of a E12.5 *PdgfbCreERT;R26mTmG*
348 hearts stained against ICAM2 (magenta). D1 boxed area shows numerous *Pdgfb*-
349 expressing endocardial sprouts (white arrowheads), some of these sprouts form bud-like
350 structures (dotted line). D2 shows the same boxed area but 90° rotated in x axis.
351 Endocardial buds (dotted line) are sprouting directly to the subepicardium.

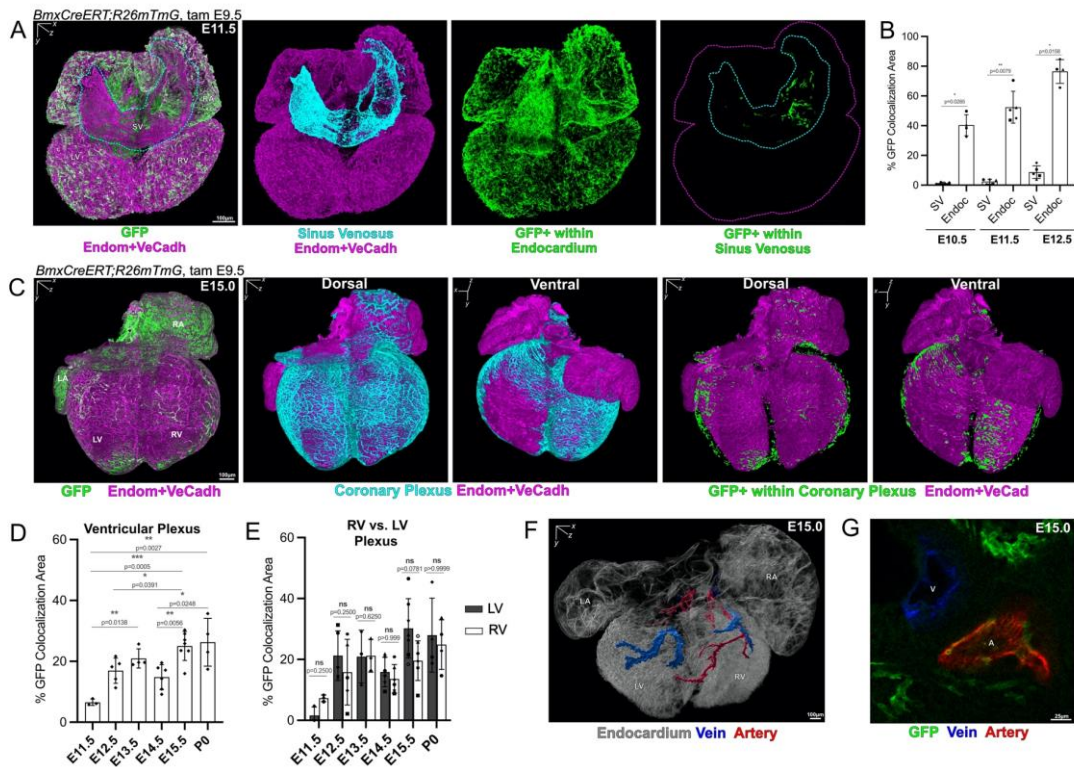
352 **E.** Three-dimensional rendering of the ventral side of a RV from a E15.5
353 *PdgfbCreERT;R26mTmG* hearts stained against ICAM2 (magenta). Subepicardial
354 plexus is progressing (dotted line) and anastomoses with the endocardial-derived
355 intramyocardial plexus. Endocardial buds are often observed (white arrowheads).

356 **F.** Quantification of endocardium expressing *Pdgfb* in the ventricles along development.
357 Quantified in every stack of a three-dimensional image as percentage of the area (μm^2)
358 of *Pdgfb*-expressing endocardial cells (GFP/Endom+VeCadherin colocalization), normalized
359 to the area of segmented endocardium (Endom+VeCadherin) of the ventricles. Data are
360 mean \pm SD, every data point (n=3, see dots on bars) is an independent individual. Non-
361 parametric Kruskal-Wallis test was performed, only significant p values are shown in
362 figure (non-significant p values are: E11.5 vs E12.5=0.8908, E11.5 vs. E14.5=0.2724,
363 E11.5 vs. E15.5=0.1200, E12.5 vs. E14.5=0.3369, E12.5 vs. E15.5=0.1563, E13.5 vs.
364 E14.5=0.1095, E13.5 vs. E15.5=0.2529, E14.5 vs. E15.5=0.6474).

365 **G.** Quantification of endocardium expressing *Pdgfb* in RV versus LV along development.
 366 Quantified as in F. Data are mean \pm SD, every data point is an independent individual
 367 (n=3, LV vs. RV, see paired dots on bars), p value by Wilcoxon rank-sum test.
 368 Intramyoc=Intramyocardial; IVS=Interventricular septum; LA=Left atrium; LV=Left
 369 ventricle; OFT=Outflow tract; RA=Right atrium; RV=Right ventricle;
 370 Subepic=Subepicardial; Tam=Tamoxifen.
 371



372
 373 **Figure S6. Endocardial tip cells show an exploratory phenotype and make contact**
 374 **with subepicardial plexus.**
 375 **A.** Dorsal view of a E12.0 *PdgfbCreERT;R26mTmG* explanted heart before (t=0) and
 376 after (t=15h) live-imaging. The dorsal coronary plexus (GFP, black) progression is
 377 comparable to the *in vivo* situation.
 378 **B.** Magnification of RV sprouting front of a E12.0 *PdgfbCreERT;R26mTmG* explanted
 379 heart before (t=0) and after (t=15h) live-imaging.
 380 **C.** Time-lapse of SV-derived plexus sprouting front over the RV. *Pdgfb*-expressing
 381 endocardial cells (red and blue arrowheads) appear actively attracted by the SV-derived
 382 plexus and finally make contact with its sprouting front.
 383 LA=Left atrium; LV=Left ventricle; RA=Right atrium; RV=Right ventricle; SV=Sinus
 384 venosus; Tam=Tamoxifen.



385
386
387
388
389
390
391
392
393
394
395
396
397
398
399
400
401
402
403
404
405
406
407
408
409
410
411
412
413
414
415
416

Figure S7. *BmxCreERT;R26mTmG* is a suitable line for endocardial tracing.

A. Three-dimensional rendering of a E11.5 *BmxCreERT;R26mTmG* heart. SV is shown in cyan, while *Bmx*-lineage cells within the SV or endocardium are shown in green. *Bmx*-lineage cells found within the SV are located close to the transition area where SV drains to RA. Single dose tamoxifen at E9.5 leads to 80% of all endocardial cells labeled at E12.5 while only 8% of SV ECs.

B. Quantification of *Bmx*-lineage cells within SV or endocardium within the tamoxifen recombination window (E9.5-E12.5). Quantified as percentage of area (μm^2) of *Bmx*-lineage cells (GFP/Endom+VeCadh colocalization), normalized to total area of corresponding segmented SV or endocardium (Endom+VeCadh). *BmxCreERT* drives labelling predominantly in the endocardium whereas minimally in the SV. Data are mean \pm SD, every data point ($n=4-5$, see dots on bars) is an independent individual, p value by Mann-Whitney U test.

C. Three-dimensional rendering of a E15.0 *BmxCreERT;R26mTmG* heart. *Bmx*-lineage derived coronary ECs (green) distribute broadly within the coronary plexus (cyan) of the ventricles.

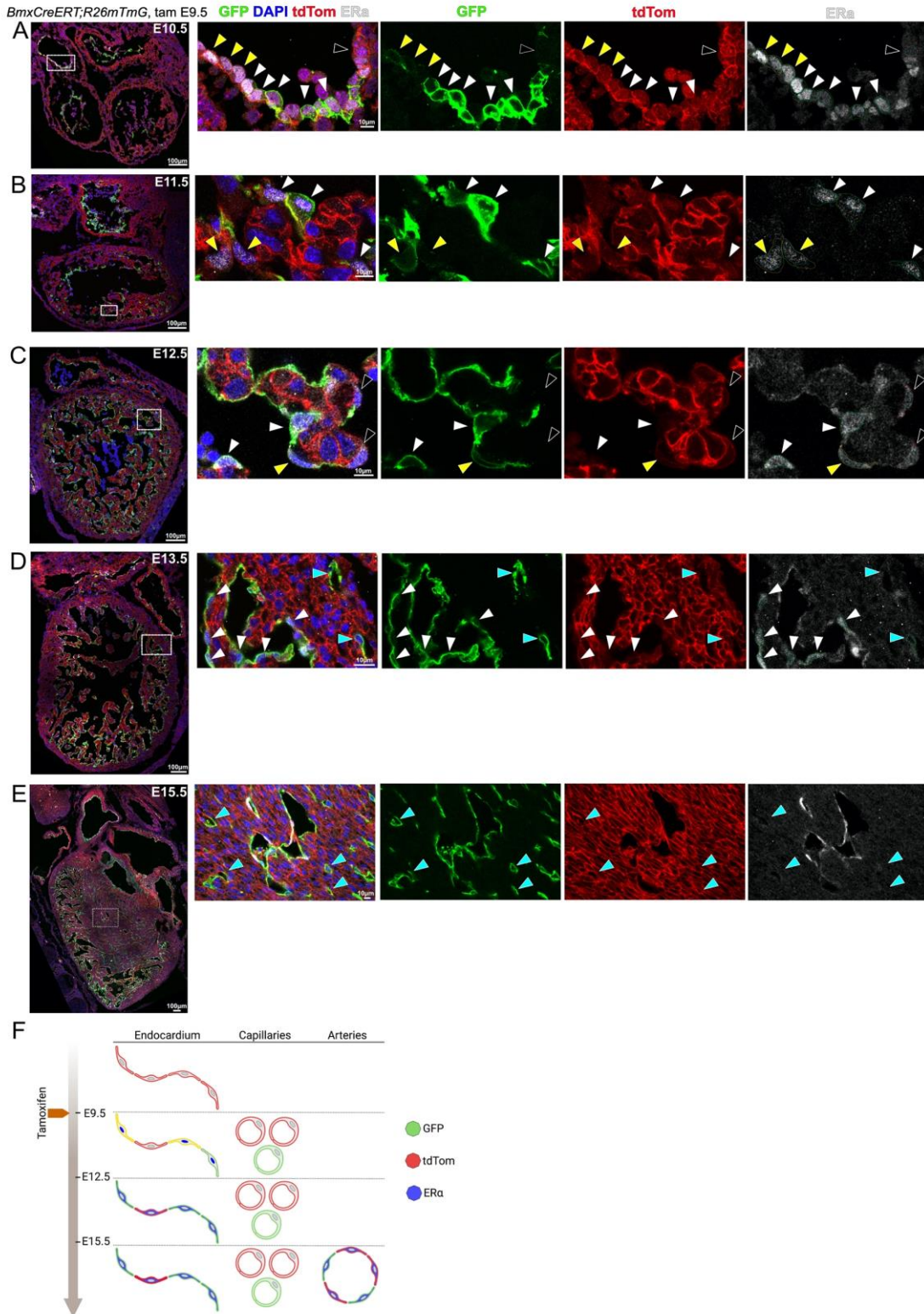
D. Quantification of *Bmx*-lineage cells within the ventricular plexus along development. Quantified in every stack of a three-dimensional image as percentage of the area (μm^2) of *Bmx*-lineage cells (GFP/Endom+VeCadh colocalization), normalized to the area of the coronary plexus of the ventricles (Endom+VeCadh). Data are mean \pm SD, every data point ($n=4-5$, see dots on bars) is an independent individual. Non-parametric Kruskal-Wallis test was performed, only significant p values are shown in figure (non-significant p values are: E11.5 vs E12.5=0.1077, E11.5 vs. E14.5=0.2338, E12.5 vs. E13.5=0.2935, E12.5 vs. E14.5=0.5826, E12.5 vs. P0=0.0962, E13.5 vs. E14.5=0.1079, E13.5 vs. E15.5=0.4218, E13.5 vs. P0=0.5609, E15.5 vs. P0=0.8829).

E. Quantification of *Bmx*-lineage cells within the plexus of LV and RV along development. Quantified in every stack of a three-dimensional image as percentage of the area (μm^2) of *Bmx*-lineage cells (GFP/Endom+VeCadh colocalization), normalized to the area of the coronary plexus of LV and RV (Endom+VeCadh). Data are mean \pm SD, every data point is an independent individual ($n=3-7$, LV vs. RV, see paired dots on bars), p value by Wilcoxon rank-sum test.

417 **F.** Post-processing segmentation of developing coronary arteries (red) and veins (blue)
 418 in a *BmxCreERT;R26mTmG* E15.5 heart. Segmentation is based in their connection to
 419 the RA through the coronary sinus (veins) or to the aorta (arteries).

420 **G.** Single z plane of heart shown in F. *Bmx*-lineage cells (green) are preferentially located
 421 integrated in coronary arteries (red) rather than coronary veins (blue).

422 A=Artery; Endoc=Endocardium; LA=Left atrium; LV=Left ventricle; RA=Right atrium;
 423 RV= Right ventricle; SV=Sinus venosus; V=Vein;



424

425 **Figure S8. *BmxCreERT* mediated recombination only occurs during a 48h time-**
 426 **window upon a single E9.5 tamoxifen injection.**

427 **A-E.** Sections of E11.5-E15.5 *BmxCreERT;R26mTmG* hearts, stained against Estrogen
 428 Receptor α ($ER\alpha$) to analyze the distribution of the CreERT (expressed from the *Bmx*
 429 promoter) and tdTomato (tdTom) proteins along development. Black arrowheads point
 430 to GFP-negative/tdTom-positive cells; yellow arrowheads to GFP-positive/tdTom-
 431 positive cells; white arrowheads to GFP-positive/tdTom-negative/ $ER\alpha$ -positive cells; and
 432 cyan arrowheads to GFP-positive/tdTom-negative/ $ER\alpha$ -negative cells.

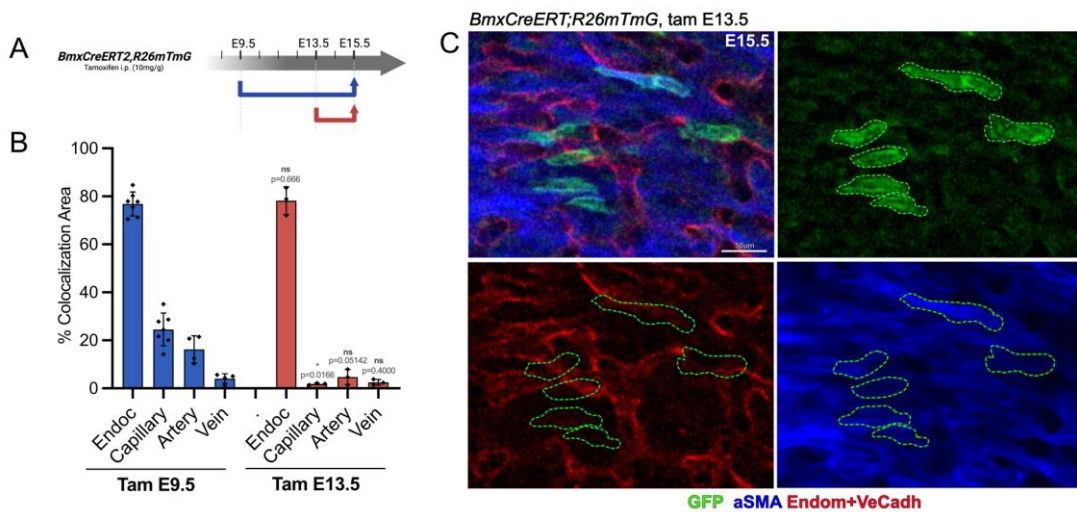
433 **F.** Schematic representation of GFP, tdTom and $ER\alpha$ signals detected in panels above.
 434 By analyzing the colocalization of GFP and tdTom we observe recombination exclusively
 435 in endocardial cells and only during the first 48h upon tamoxifen administration. Also, in
 436 this time window, $ER\alpha$ localizes to the nuclei of *Bmx*-expressing endocardial cells. From
 437 E12.5 onwards, $ER\alpha$ is found in the cytoplasm of all *Bmx*-expressing endocardial cells.
 438 In capillaries, we never observe CreERT or tdTom expression, indicating that GFP
 439 labeling is evidence for being derived from the *Bmx*-lineage endocardium.

440 In arteries, we detect $ER\alpha$ expression, which recapitulates *Bmx* expression. However,
 441 $ER\alpha$ is always located at the cytoplasm, so the GFP labeling in arterial ECs is not due
 442 to autonomous recombination in arteries, but a consequence of earlier lineage
 443 recombination (as endocardial cells). Also, we observe $ER\alpha$ -expressing arterial cells that
 444 lack GFP, providing further evidence that the earlier tamoxifen injection is no-longer
 445 leading to any recombination event at this later stage.

446 Tam=Tamoxifen.

447

448



449

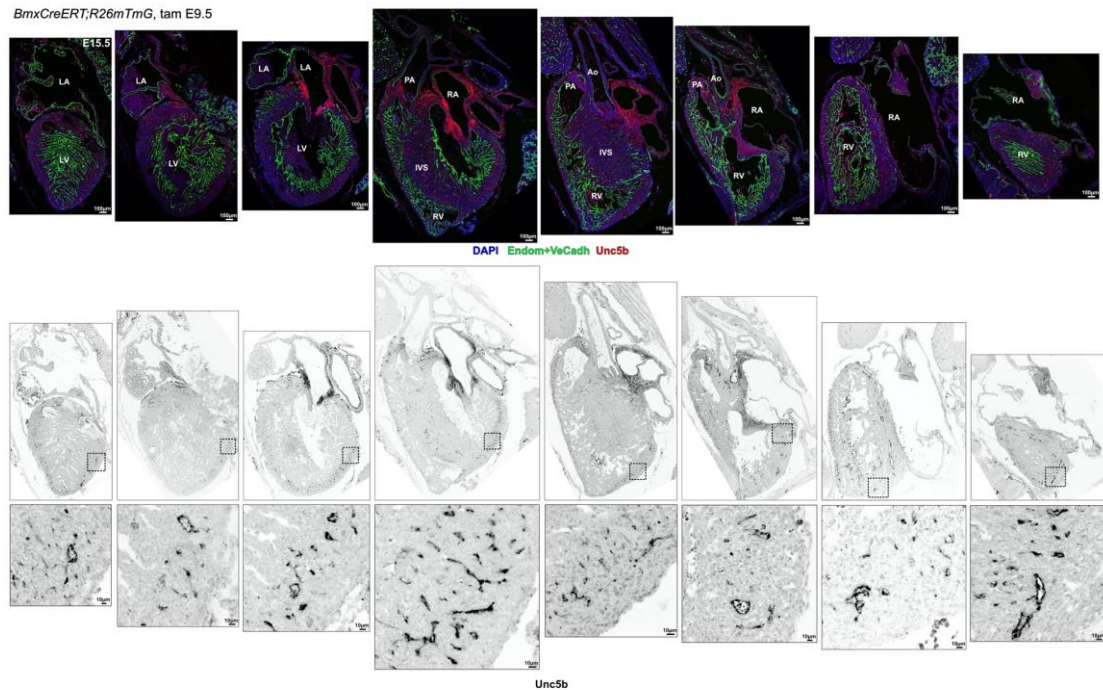
450 **Figure S9. *Bmx* is not upregulated by ECs within the *BmxCreERT* recombination**
 451 **window upon a single E9.5 tamoxifen injection.**

452 **A.** Lineage-tracing strategy. Comparison of E15.5 *BmxCreERT;R26mTmG* hearts when
 453 tamoxifen is administered at different timepoints (E9.5 and E13.5).

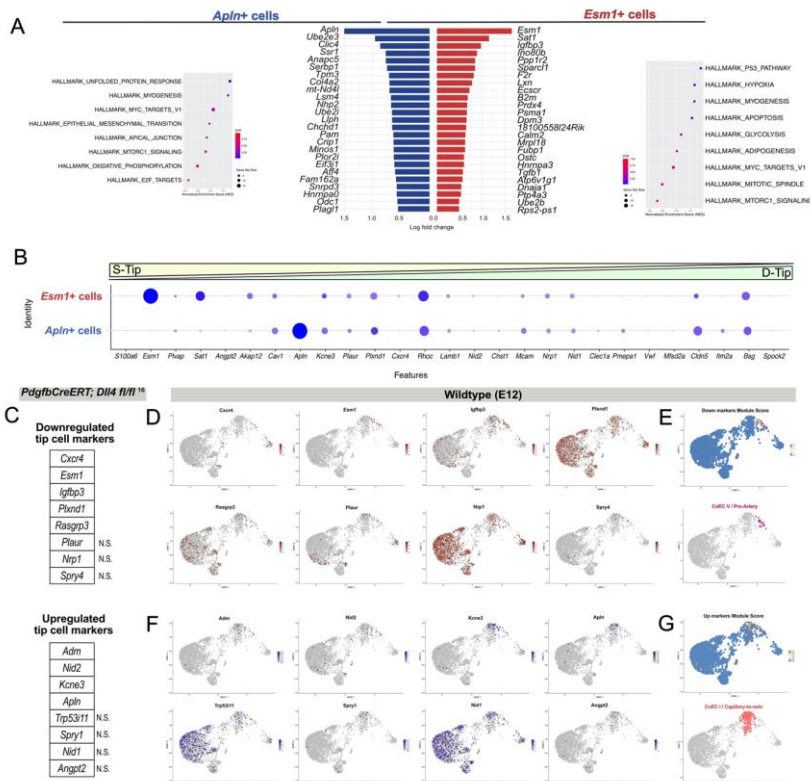
454 **B.** Percentage of *Bmx*-lineage cells within endocardium or coronary plexus, segmented
 455 in capillaries, arteries or veins at E15.5. Quantified in every stack of a three-dimensional
 456 image as GFP/Endom+VeCadh colocalization area (μm^2), normalized to the area of
 457 segmented capillaries, arteries or veins. E13.5 tamoxifen administration leads to a
 458 decreased labeling of *Bmx*-lineage derived coronary plexus. Data are mean \pm SD, every
 459 data point (n=3-7, see dots on bars) is an independent individual, p value by Mann-
 460 Whitney U test.

461 **C.** Section of a E15.5 *BmxCreERT;R26mTmG* heart, stained against α SMA and
 462 Endom+VeCadh. Only when tamoxifen is administered at E13.5, *Bmx*-lineage non-

463 endothelial cells are observed (green outline), confirming that E9.5 single-dose
 464 tamoxifen does not lead to any recombination 72 hours later (at E13.5).
 465 Endoc=Endocardium, Tam=Tamoxifen.
 466



467
 468 **Figure S10. Unc5b-expressing pre-arterial cells localize in the intramyocardial**
 469 **segment.**
 470 **A.** Left-to-right serial sections of a E15.5 *BmxCreERT;R26mTmG* heart, stained against
 471 Unc5b (red), Endom+VeCadh (green) and DAPI (blue). In the bottom panel, Unc5b
 472 expression is shown in gray scale for better visualization. Boxed areas show a
 473 magnification of panel above. Unc5b is expressed by the intramyocardial plexus and by
 474 vessels that showed signs of arterialization.
 475 Ao=Aorta; IVS=Interventricular septum; LA=Left atrium; LV=Left ventricle;
 476 PA=Pulmonary artery; RA=Right atrium; RV=Right ventricle; Tam=Tamoxifen.
 477



478
479
480
481
482
483
484
485
486
487
488
489
490
491
492
493
494
495

Figure S11. Differential transcriptional signature of *Esm1*-expressing and *Apln*-expressing tip cell subpopulation.

A. DEGs between *Apln*-expressing and *Esm1*-expressing tip cells and corresponding gene set enrichment analysis for hallmarks of each population at E12. *Esm1*-expressing tip cells show enrichment of p53 and hypoxia pathways genes.

B. Dotplot of expression level and frequency of transcriptional signatures described for S-Tip and D-Tip subpopulations in the retina⁴⁷. No clear correlation is detected between retina and cardiac tip cell subpopulations.

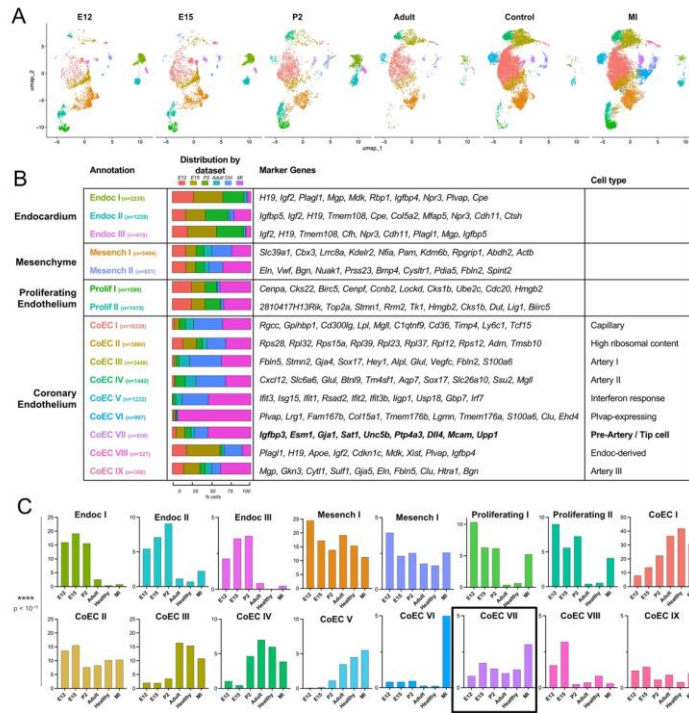
C. List of tip cell marker genes described as down- or up-regulated in cardiac *Pdgfrb*-expressing ECs upon 24 hours *Dll4* deletion¹⁶.

D. Feature marker plots of downregulated markers at E12 in the integrated UMAP.

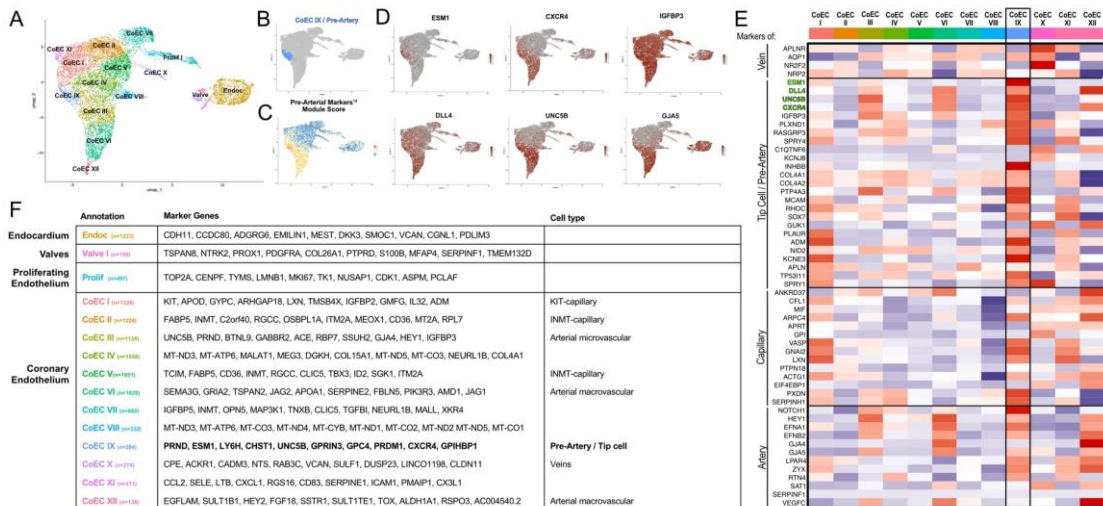
E. Module score for significantly downregulated markers upon *Dll4* loss shows enrichment in the CoEC V/Pre-Artery cluster.

F. Feature marker plots of upregulated markers at E12 in the integrated UMAP.

G. Module score for significantly upregulated markers upon *Dll4* loss shows enrichment in the CoEC I/Capillary-to-vein cluster.



496
 497 **Figure S12. Cluster annotation and distribution of E12, E15, P2, Adult, Control and**
 498 **MI integrated dataset.**
 499 **A.** UMAP plot with annotated cluster split by dataset of origin.
 500 **B.** Annotations and cell number of every cluster (first row), with their distribution
 501 throughout the different developmental stages (second row), top 10 marker genes (third
 502 row) and the assigned cell type.
 503 **C.** Percentage of every cluster in each dataset, normalized by total cell number. CoEC
 504 VII / Pre-Artery clusters proportion is increased in response to myocardial infarction. P
 505 value by Chi-square test.
 506



507
 508 **Figure S13. Pre-arterial cell population with tip cell signature is detected in human**
 509 **embryos.**
 510 **A.** UMAP plot with annotated cluster split by dataset of origin.
 511 **B.** UMAP plot showing CoEC IX cluster highlighted in blue.

512 **C.** Module score of previously described pre-arterial marker genes¹¹. CoEC IX shows a
513 high score for this set of genes.

514 **D.** Feature marker plot of pre-arterial and tip cell markers (*Esm1*, *Cxcr4*, *Igfbp3*, *Dll4*,
515 *Unc5b*) and arterial marker (*Gja5*).

516 **E.** Heatmap of a wide list of known venous, tip cell, capillary and arterial markers in all
517 coronary ECs clusters (CoEC I to CoEC IX).

518 **F.** Annotations and cell number of every cluster (first row), with their distribution
519 throughout the different developmental stages (second row), top 10 marker genes (third
520 row) and the assigned cell type.

521

522

523 **Supplementary tables' legends**

524

525 **Table S1. Source data of figures 1D, 3G, 3H, 4C, 5D, S2C, S4G, S5F, S5G, S7B, S7D,**
526 **S7E, S9B, S12B, S12C, S13**

527

528 **Table S2. Complete list of differentially expressed genes of figures 1D, S11A, S13F**

529

530

531 **Supplementary videos' legends**

532

533 **Movie S1. Supplemental to Figure S5A.**

534 Three-dimensional rendering of a E11.5 *PdgfbCreERT;R26mTmG* heart. GFP (green),
535 Endom+VeCadh (magenta).

536

537 **Movie S2. Supplemental to Figure S5A.**

538 Three-dimensional rendering of a E12.5 *PdgfbCreERT;R26mTmG* heart. GFP (green),
539 Endom+VeCadh (magenta).

540

541 **Movie S3. Supplemental to Figure S5A.**

542 Three-dimensional rendering of a E13.5 *PdgfbCreERT;R26mTmG* heart. GFP (green),
543 Endom+VeCadh (magenta).

544

545 **Movie S4. Supplemental to Figure S5A.**

546 Three-dimensional rendering of a E14.5 *PdgfbCreERT;R26mTmG* heart. GFP (green),
547 Endom+VeCadh (magenta).

548

549 **Movie S5. Supplemental to Figure S5A.**

550 Three-dimensional rendering of a E15.5 *PdgfbCreERT;R26mTmG* heart. GFP (green),
551 Endom+VeCadh (magenta).

552

553 **Movie S6. Supplemental to Figure S5C.**

554 Three-dimensional rendering of a E11.5 *PdgfbCreERT;R26mTmG* heart, magnification
555 of the interventricular septum. GFP(green), Endom+VeCadh (magenta).

556

557 **Movie S7. Supplemental to Figure S5D.**

558 Three-dimensional rendering of a E12.5 *PdgfbCreERT;R26mTmG* heart, magnification
559 of the interventricular septum. GFP(green), Endom+VeCadh (magenta).

560

561 **Movie S8. Supplemental to Figure S5D1-D2.**

562 Three-dimensional rendering of a E12.5 *PdgfbCreERT;R26mTmG* heart, magnification
563 of movie 11. GFP(green), Endom+VeCadh (magenta).

564

565 **Movie S9. Supplemental to Figure S5E.**

566 Three-dimensional rendering of a E15.5 *PdgfbCreERT;R26mTmG* heart, magnification
567 of the ventral side of the right ventricle. GFP(green), Endom+VeCadh (magenta).

568

569 **MovieS10. Supplemental to Figure 2C.**

570 Three-dimensional rendering of a E11.5 *PdgfbCreERT;R26mTmG* heart, magnification
571 of the SV-derived plexus sprouting front. Segmented SV and SV-derived plexus (cyan),
572 GFP+ within the endocardium (green).

573

574 **Movie S11. Supplemental to Figure S6.**

575 Time-lapse of a E12.5 *PdgfbCreERT;R26mTmG* heart, magnification of the right
576 ventricle SV-derived plexus sprouting front. GFP (black).

577

578 **Movie S12 - Supplemental to Figure 2F**

579 Three-dimensional rendering of a E11.5 *PdgfbCreERT;R26mTmG* heart, magnification
580 of the atrioventricular canal. GFP (green), Endom+VeCadh (magenta).

581

582 **Movie S13. Supplemental to Figure S7A.**

583 Three-dimensional rendering of a E11.5 *BmxCreERT;R26mTmG* heart. GFP (green),
584 Endom+VeCadh (magenta).

585

586 **Movie S14. Supplemental to Figure S7C.**

587 Three-dimensional rendering of a E15.0 *BmxCreERT;R26mTmG* heart. GFP+ cells
588 within the coronary plexus(green), Endom+VeCadh (magenta).

589

590 **Movie S15. Supplemental to Figure S7F.**

591 Three-dimensional rendering of a E15.0 heart. Veins and arteries are shown in blue and
592 red respectively, and endocardium in gray.

593

594 **Movie S16. Supplemental to Figure 4D1.**

595 Three-dimensional rendering of a E13.5 *Esm1CreERT;R26mTmG* heart, magnification
596 of the sprouting front of the subepicardial plexus. GFP(green), Endom+VeCadh
597 (magenta).

598

599 **Movie S17. Supplemental to Figure 4D2.**

600 Three-dimensional rendering of a E13.5 *Esm1CreERT;R26mTmG* heart, magnification
601 of the myocardial wall of LV. GFP(green), Endom+VeCadh (magenta).

602

603 **Movie S18. Supplemental to Figure 4D3.**

604 Three-dimensional rendering of a E13.5 *Esm1CreERT;R26mTmG* heart, magnification
605 of the subendocardial zone of LV. GFP(green), Endom+VeCadh (magenta).

606

607 **Movie S19. Supplemental to Figure 4D4.**

608 Three-dimensional rendering of a E13.5 *Esm1CreERT;R26mTmG* heart, magnification
609 of the interventricular septum. GFP(green), Endom+VeCadh (magenta).

610

611 **Movie S20. Supplemental to Figure 4D5.**

612 Three-dimensional rendering of a E13.5 *Esm1CreERT;R26mTmG* heart, magnification
613 of the aortic root. GFP(green), Endom+VeCadh (magenta).

614

615 **Movie S21. Supplemental to Figure 4F3.**

616 Three-dimensional rendering of a E18.5 *Esm1CreERT;R26mTmG* heart, magnification
617 subendocardial zone of the LV. GFP(green), Endom+VeCadh (magenta).